Vol. 1, 1991, pp. 17–25.
[3]Bruckner, A. P., Knowlen, C., Hertzberg, A., and Bogdanoff, D. W., "Operational Characteristics of the Thermally Choked Ram Accelerator," *Journal of Propulsion and Power*, Vol. 7, 1991, pp. 828–836.
[4]Seiler, F., Patz, G., Smeets, G., and Srulijes, J., "Status of ISL's RAMAC 30 with Rail Stabilized Projectiles," 1st International Workshop on Ram Accelerator, Saint-Louis, France, Sept. 1993.
[5]Chang, X., Kanemoto, H., and Taki, S., "A Ram Accelerator with Rectangular Bore is Working at Hiroshima University," AIAA Paper 95-2496, July 1995.
[6]Bruckner, A. P., Burnham, E. A., Knowlen, C., Hertzberg, A., and Bogdanoff, D. W., "Initiation of Combustion in the Thermally Choked Ram Accelerator," *Shock Waves, Proceedings of the 18th International Symposium on Shock Waves*, edited by K. Takayama, Springer–Verlag, Berlin, 1992, pp. 623–630.
[7]Knowlen, C., and Bruckner, A. P., "Hugoniot Analysis of the Ram Accelerator," *Shock Waves, Proceedings of the 18th International Symposium on Shock Waves*, edited by K. Takayama, Springer–Verlag, Berlin, 1992, pp. 617–622.

Further Examination of Enthalpy Rocket Performance

Merrill K. King*
NASA Headquarters, Washington, D.C. 20546

Introduction

PARKER and Humble[1] examined the potential performance of enthalpy rocket propulsion, based on the transfer of stored thermal energy from an inert metal or ceramic capacitor into a nonreacting working fluid; Gany[2] also examined this concept. In these analyses, the thermal capacitor material was assumed to begin as a liquid at its melting point and end as a solid, also at the melting point. In addition, the total mass of the system was assumed to consist of the capacitor and working fluid masses, with no additional inerts or payload other than the capacitor itself. Parker and Humble[1] took a somewhat convoluted approach to arriving at their final expression for velocity increment ΔV, which can easily be shown to reduce to the standard velocity increment equation

$$\Delta V = I_{sp} g_c \, \ell n[(m_{cap} + m_{WF})/m_{cap}] \tag{1}$$

where I_{sp} is the specific impulse of the working fluid at the melting temperature of the capacitor material, m_{cap} is the mass of the thermal capacitor, and m_{WF} is the total mass of the working fluid, with the two masses being related by the heat required to raise the working fluid from its initial temperature (not defined in Ref. 1) to the capacitor melting temperature. Gany[2] recognized the equivalence of Eq. (1) for this analysis and used it to derive a velocity increment equation utilizing idealized equations for the working fluid expansion process and setting the total latent energy storage of the capacitor equal to the heat required to raise the working fluid to the capacitor melting temperature by means of Eq. (3) of Ref. 2: $m_{cap}\Delta Q_{melt} = m_{WF} c_p T_{melt}$. Implicit in the previously mentioned Eq. (3) is the assumption that the working fluid is initially at absolute zero temperature and that there are no latent heats associated with heating this fluid from absolute zero to the capacitor melt temperature.

Received Feb. 6, 1997; revision received July 28, 1997; accepted for publication July 29, 1997.

*Enterprise Scientist, Microgravity Combustion, Code UG, 300 E Street SW. Fellow AIAA.

In the analysis presented here, whose main contribution will be to examine the effects of using the thermal capacitor more completely by allowing it to start at temperatures well above its melting point and end at temperatures well below it, and the effects of different means of staging working fluid flow through the capacitor, most of the results will assume initial working fluid conditions as gas at 273 K; a brief examination of more realistic initial conditions is presented at the end of this note. Equation (1) was used as the starting point in this analysis, with the specific impulse of the working fluid (for infinite expansion ratio and a zero-back-pressure environment) being calculated from

$$I_{sp} = (2c_p T_0/g)^{1/2} = [2\gamma R/g(\gamma - 1)]^{1/2}(T_0/MW)^{1/2} \tag{2}$$

where $\gamma = 1.4$ for a diatomic working gas and 1.667 for a monoatomic gas, T_0 is the working fluid total temperature after heat exchange with the capacitor, and MW is the molecular weight of the working fluid. The relationship between working fluid and capacitor masses is obtained by equating the latent heat stored in the capacitor to the heat required to raise the working fluid from its initial temperature to the capacitor melting point, resulting in

$$m_{WF} = [\Delta Q_{melt}/c_p(T_{melt} - T_{init})]m_{cap} \tag{3}$$

$$\Delta V = I_{sp} g_c \, \ell n[1 + \Delta Q_{melt}/c_p(T_{melt} - T_{init})] \tag{4}$$

Velocity increment values calculated by Parker and Humble,[1] Gany,[2] and by the use of Eqs. (2–4) are presented for several combinations of working fluid and thermal capacitor material for the scenario where only fusion heat is extracted from the capacitor in Table 1. There are significant differences in absolute values calculated, resulting from the different initial conditions assumed for the working fluid. Because of the nonlinear interactions between various working fluid and capacitor properties, these differences do not show up as constant ratios; the differences are particularly pronounced for the lithium capacitor because its low melting temperature makes it particularly sensitive to different initial working fluid temperature assumptions through the $(T_{melt} - T_{init})$ term in Eqs. (3) and (4). (Note that working fluid initial conditions are not specified by Parker and Humble[1]; part of the differences appearing in Table 1 may result from their using conditions other than gas at 273 K.)

As indicated, one purpose of this study was to evaluate additional velocity increment potential associated with using specific heat storage as well as the latent heat storage capacity of the capacitor materials; relevant properties for several attractive candidates are presented in Table 2. (The peak operating temperatures listed in Table 2 are somewhat arbitrary, being chosen to be sufficiently lower than the boiling points to minimize carrier vaporization problems.) It is particularly instructive to compare columns 5, 7, and 8 of Table 2. Column 5 gives the latent heat available per gram of material, column 7 gives the total heat storage between the peak temperature and the solidus end of the melting point, and column 8 gives the total heat storage between the peak temperature and 500 K; the total storage capability is much larger than the latent heat storage capacity, suggesting further examination of the enthalpy rocket concept using some or all of this additional capacity.

The procedure used to examine this potential is outlined next; in this phase of the study, it was assumed that all working fluid passes through the entire capacitor bed, with the isothermal bed temperature decreasing with time. First, a basis weight of capacitor material was chosen. A small temperature decrement from the initial peak temperature was selected and the amount of working fluid mass passing through the capacitor associated with this decrement was calculated as

$$m_{WF,j} = (\text{Basis Wt})c_{p,cap}\Delta T_j/c_{p,WF}(T_{av,j} - 273) \tag{5}$$

Table 1 Velocity increment m/s for various working fluids through various thermal capacitor materials, using only latent heat of melting

Capacitor material	Working fluid				Reference
	Hydrogen	Oxygen	Argon	Nitrogen	
Lithium	572	1202	1102	1196	1
	343	864	917	——	2
	755	1421	1400	1417	Present study
Magnesium oxide	339	1016	1233	1007	1
	389	1187	1426	——	2
	451	1362	1524	1315	Present study
Beryllium	300	866	987	859	1
	——	——	——	——	2
	377	1102	1226	1068	Present study
Boron	416	1171	1360	1163	1
	396	1331	1538	——	2
	539	1514	1658	1472	Present study
Beryllium oxide	507	1396	1623	1392	1
	579	1619	1848	——	2
	672	1815	1966	1767	Present study

Table 2 Relevant properties of candidate thermal capacitor materials

Material	MP, K	BP, K	Peak T, K	Δh_{melt}, cal/gm	c_p, cal/gm K	Heat storage A[a]	Heat storage B[b]
Lithium	477	1615	1500	158	0.85	1027	1027
Boron	2377	2823	2500	490	0.245	520	980
Beryllium	1576	3243	3000	260	0.44	887	1360
BeO	2832	>4000	3500	680	0.24	840	1400
MgO	2915	3900	3000	459	0.225	591	1134

[a]Heat storage A = latent heat of fusion plus sensible heat change from peak temperature to melting temperature.
[b]Heat storage B = latent heat of fusion plus sensible heat change from peak temperature to 500 K.

where $c_{p,\mathrm{WF}} = (R/MW_{\mathrm{WF}})\ [\gamma/(\gamma - 1)]$. Equation (2) was used to calculate an average specific impulse for this working fluid increment. This procedure was repeated until the melting point of the capacitor material was reached, at which point a working fluid mass associated with the solidification was calculated using Eq. (3), with Eq. (2) being used to calculate specific impulse for this increment with $T = T_{\mathrm{melt}}$. Subsequent to solidification, further temperature increments were calculated as before until the specified final capacitor temperature was reached. The total mass of working fluid was then calculated as the sum of all the incremental values, and initial and final system masses associated with expulsion of each increment of working fluid ($m_{\mathrm{Inc,init}}$ and $m_{\mathrm{Inc,final}}$) were calculated in a straightforward manner. Finally, total velocity increment associated with expulsion of all of the working fluid was calculated as

$$\Delta V = \sum \Delta V_j + \Delta V_{\mathrm{solidification}} = g_c \sum I_{\mathrm{sp}}\, \ell n(m_{\mathrm{inc,init}}/m_{\mathrm{inc,final}}) \tag{6}$$

First, several cases with use of the total heat available between the peak temperature and the solidus end of the melt temperature were examined. For hydrogen plus beryllium, the total velocity increment was found to increase from 377 (Table 1) to 990 m/s, for hydrogen plus lithium it increased from 752 to 2207 m/s, for argon plus beryllium it increased from 1226 to 2262 m/s, and for argon plus lithium it increased from 1400 to 2258 m/s, significant increases in all cases. Next, a series of cases in which the thermal capacitor was depleted from peak temperature down to approximately 500 K (arbitrary cutoff, based on significant violation of the constant specific heat ratio approximation at lower temperatures) was examined; in general, an optimum bottom temperature in the 600–1000 K range was found. The best combinations of working fluid and thermal capacitor materials among those examined were argon + BeO (2440 m/s), argon + Be (2470 m/s), and nitrogen + Be (2620 m/s).

Next, a brief study of another scenario, in which successive infinitesimal increments of working fluid are passed through different (thermally isolated) incremental fractions of the bed,

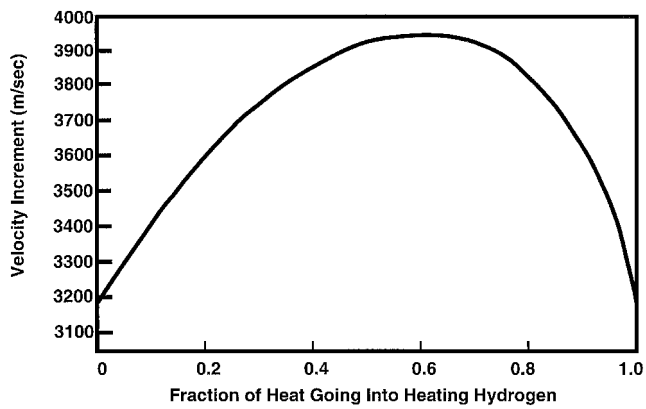

Fig. 1 Velocity increment vs fraction of heat transferred into hydrogen (vs nitrogen) for scenario in which all gas increments leave thermal capacitor at 600 K.

such that all gas is expelled at an arbitrarily chosen bottom temperature, was carried out. This scenario results in a lower specific impulse but in larger quantities of working fluid per unit mass of capacitor (since all of the working fluid is heated only to the bottom temperature), thus decreasing the I_{sp} part of Eq. (1), but increasing the magnitude of the log term. (600 K was chosen as the bottom temperature for these cases; one could obviously perform calculations for lower temperatures down to 273 K, resulting in an infinite velocity increment, but requiring an infinite amount of working fluid for the specified nonzero capacitor mass, an impractical situation.) With nitrogen, the resulting specific impulse is 113.95 s, while the mass ratio of nitrogen to capacitor (beryllium) is 16.23, leading to $\Delta V = 113.95\ (9.8)\ell n(17.23) = 3180$ m/s. With hydrogen, the specific impulse is 426.1 s, whereas the mass ratio of working fluid to capacitor is 1.159, leading to $\Delta V = 426.1\ (9.8)\ell n(2.159) = 3214$ m/s. Within this scenario, the possibility of using nitrogen to extract heat early in the process, with a changeover to hydrogen as a working fluid in later stages, was

also examined, with the results depicted in Fig. 1, where total velocity increment is plotted against fraction of total available heat going to the hydrogen. As may be seen, this procedure can result in significant increases from the velocity increments found for either working fluid alone, with a maximum velocity increment of nearly 4000 m/s being achieved when approximately two-thirds of the heat is extracted by hydrogen.

Finally, one degree of realism was imposed with calculations using initial conditions for the working fluids as liquid hydrogen at 20 K and liquid nitrogen at 90 K. This required straightforward modification of the calculation of working fluid/capacitor mass ratios with the use of modified initial temperatures in Eq. (3) and the inclusion of an additional term in that equation to account for the heat of vaporization of the working fluids. Under these conditions, the maximum velocity increment attained was reduced to 2650 m/s, with the optimum nitrogen/hydrogen split being approximately 45/55. Obviously, further calculations using more realistic working fluid initial conditions, including inert masses for tankage and useful payload weights must be performed if one is to pursue this enthalpy rocket approach further.

References

[1]Parker, T. W., and Humble, R. W., "Theoretical Upper Limits on Enthalpy Rocket Performance," *Journal of Propulsion and Power*, Vol. 12, No. 2, 1996, pp. 445–448.

[2]Gany, A., "Comment on 'Theoretical Upper Limits on Enthalpy Rocket Performance,'" *Journal of Propulsion and Power*, Vol. 13, No. 1, 1997, pp. 167, 168.

Effects of Kinetic Rate Uncertainty on the Predicted Performance of Solar Thermal Rockets

D. Brian Landrum* and Robert M. Beard†
University of Alabama in Huntsville, Huntsville, Alabama 35899

Introduction

SOLAR thermal propulsion has emerged as a candidate for future orbital transfer vehicles. In a solar thermal rocket, reflectors concentrate solar energy into an absorber that heats the propellant. Because of hydrogen's low molecular weight, a hydrogen-fueled solar thermal rocket operating at typical absorber temperatures of 2220–3390 K (4000–6100°R) can theoretically produce specific impulses I_{sp} of 700–1200 s. Previous research indicates that the actual I_{sp} delivered by solar thermal rockets is significantly lower than the predicted ideal value.[1] Therefore, accurate predictions of nonideal nozzle performance are essential to the development of these low-thrust systems.

Presented as Paper 96-2856 at the AIAA/ASME/SAE/ASEE 32nd Joint Propulsion Conference, Lake Buena Vista, FL, July 1–3, 1996; received May 5, 1997; revision received July 16, 1997; accepted for publication Aug. 2, 1997.

*Assistant Professor, Propulsion Research Center, Department of Mechanical and Aerospace Engineering, RI E-33. Senior Member AIAA.

†Graduate Research Assistant, Propulsion Research Center, Department of Mechanical and Aerospace Engineering, RI E-32. Student Member AIAA.

Specific impulse losses are caused by flow divergence, viscous losses, and finite rate chemical kinetics.[2] As the hydrogen is heated in the absorber, the thermal energy input causes a fraction of the gas molecules to dissociate. The short residence time of the expanding gas in the small nozzle does not permit full chemical equilibrium to be reached. The magnitude of nonequilibrium is determined by the hydrogen recombination rate, which is a function of the chamber temperature and pressure, the divergent nozzle geometry, and the rate constant. A research literature review revealed hydrogen recombination rate constant variations of as much as two orders of magnitude.[3,4] Depending on the chamber conditions and the particular rate model chosen, this uncertainty could have a significant impact on solar thermal rocket performance predictions. The results of this study are applicable to the design of small-scale thrusters that use hot hydrogen propellant.

Hydrogen Kinetics

The exothermic recombination of hydrogen is governed by two reactions

$$\mathrm{H} + \mathrm{H} + M_i \overset{k_i}{\Rightarrow} \mathrm{H}_2 + M_i \tag{1}$$

where M_i is either an atomic H or molecular H_2 third-body. The rate constant of each reaction can be written in the Arrhenius form

$$k_i = A_i T^{N_i} \cdot \exp(-E_{ai}/RT) \tag{2}$$

A broad range of experimentally and analytically determined values for k_{H_2} and k_H are presented in the research literature.[3–7] Wetzel and Solomon[4] studied the impact of rate uncertainty on the performance of high-thrust (~44.5 kN or 10,000 lbf) nuclear thermal rockets, and defined a set of high, nominal, and low rates. The Warnatz recommended rate set was chosen for NASP propulsion technology research.[5] Baulch et al.[6] recommended a set of widely used rates. Cohen and Westberg[7] also defined a set of high, nominal, and low rates. The various rate constants are presented graphically vs temperature in Figs. 1 and 2. Also shown are hydrogen recombination rates used in the NASA-developed, finite difference Navier–Stokes (FDNS) code[8] and the two-dimensional kinetics (TDK) code.[9] In the temperature range of interest in the present study, the rate constant values vary by as much as two orders of magnitude.

Numerical Model

The numerical simulations were performed with the CFD-ACE™ code.[10] The code uses a finite volume, pressure-based method to solve the Favre-averaged Navier–Stokes equations as a system of scalar transport equations in strongly conservative form

$$\frac{\partial \rho_\phi}{\partial t} + \frac{\partial}{\partial x_\beta}(\rho u_\beta \phi) = \frac{\partial}{\partial x_\beta}\left(\Gamma_\phi \frac{\partial \phi}{\partial x_\beta}\right) + S_\phi \tag{3}$$

where ρ is the density, u_β are the velocity components, Γ_ϕ is the effective diffusion coefficient, and S_ϕ is the scalar source term. An underrelaxed, implicit iterative procedure is used to solve steady-state problems. A hybrid, central-upwind scheme is used for the spatial differencing to model mixed subsonic/supersonic flow regimes typical of rocket nozzles. A SIMPLEC algorithm was chosen for the pressure-velocity coupling. Equilibrium, finite rate, and frozen chemistry can be modeled. The second author developed a postprocessing program that integrates the calculated properties across the nozzle exit to determine thrust, mass flow rate, and I_{sp}.

The nozzle had a 1.58 mm (0.06215 in.) throat radius, a divergent area ratio of 100:1, a convergent area ratio of 35:1,